INSTITUTE OF PHYSICS PUBLISHING SEMICONDUCTOR SCIENCE AND TECHNOLOGY

Semicond. Sci. Technol. **21** (2006) 979–986 doi:10.1088/0268-1242/21/7/026

Modelling of grain boundary effects in nanocrystalline/multicrystalline silicon heterojunction solar cells

Mahdi Farrokh-Baroughi and Siva Sivoththaman

Department of Electrical and Computer Engineering, University of Waterloo, 200 University Avenue West, Waterloo, Ontario N2L 3G1, Canada

E-mail: mfarrokh@uwaterloo.ca and sivoththaman@uwaterloo.ca

Received 22 December 2005, in final form 25 April 2006
Published 14 June 2006
Online at stacks.iop.org/SST/21/979

Abstract

Heterojunction solar cells formed by nanocrystalline silicon films on fine-grained multicrystalline silicon substrates are simulated in the presence of grain boundaries. The effects of grain boundaries on the dark and illuminated current–voltage (I–V) characteristics and spectral response (SR) of heterojunction (HJ) solar cells are assessed using 1D and 2D device simulations. The grain boundary in fine-grained multicrystalline silicon is modelled in two ways: as a defective surface with continuous defect distribution throughout the bandgap, and as a hypothetical sheet with a certain recombination velocity for electrons and holes. The SR and I–V characteristics of HJs are exploited to characterize grain boundary effects on the photovoltaic properties of the solar cells and photodetectors. Simulation results show noticeable differences on the dark I–V and SR of on- and off-grain boundary HJs. Grain boundary effects become important when fine-grained multicrystalline substrates are used. Measurement results of tiny test structures fabricated on the grain boundary show consistently inferior dark I–V and SR characteristics compared to those fabricated away from the grain and allow us to quantify the recombination at the grain boundary.

1. Introduction

Material cost reduction is an important issue in the fabrication of silicon (Si) photovoltaic (PV) cells, because the material cost accounts for nearly half of the overall PV module cost. Multicrystalline silicon (mc-Si), silicon ribbons and related materials offer a cost-effective option for Si PV cells compared with single crystalline Si [1]. In most of those materials, however, the presence of a large number of grain boundaries (GBs) and crystallographic defects necessitates defect passivation. For example, defect passivation by atomic hydrogen is a very efficient technique for low-quality mc-Si substrates [2, 3]. However, in order to preserve the passivation, any post-passivation process must not be at high temperatures. Formation of heterojunctions (HJs) such as amorphous/crystalline Si [4] provided a low-temperature (LT) option for solar cell fabrication. Recently, nanocrystalline Si (nc-Si)/mc-Si HJs have been used to fabricate solar cells using small-grained mc-Si substrates [5]. A nc-Si/c-Si heterojunction is expected to result in a better long-term stability than a-Si/c-Si HJ solar cells because of a-Si degradation due to the Stabler–Wronski effect. Further, the high mobility values possible in nc-Si lead to films with high conductivity, potentially eliminating the need for transparent conductive oxides.

The grain sizes of Si materials for solar cells range from large grains, e.g., edge-defined-film-growth (EFG) Si [6] (cm^2 range) and cast mc-Si (mm^2 to cm^2 range), to much finer grains, e.g., ribbon-growth-on-substrate (RGS) Si [7] (sub-mm^2 range), and electromagnetically cast (EMC) mc-Si [8] (mm^2 range). GBs include trap centres that can act as generation–recombination centres, potentially degrading the short circuit current by recombining photogenerated carriers and fill factor and open circuit voltage by increasing the diode leakage current. GB effects in solar cells become important for fine-grained Si wafers. For example, while EMC mc-Si is

attractive because of the low oxygen and impurity content due to the EMC method, the small grain sizes (i.e., high density of GBs) necessitate an effective grain boundary passivation.

Extensive theoretical and experimental work has been performed on GBs in polycrystalline- and mc-Si, mainly to investigate carrier transport and recombination [9–11]. Complex analytical models for vertical GBs in classical pn junction solar cells have been presented [12]. Modelling complexity originates from the 2D nature of the structure and the presence of GB defects. Since LT HJ processes are ideally suited for defective substrates, a clear understanding of the GB effects on the HJ is necessary. Analytical modelling of nc-Si/mc-Si HJ on a GB is even more complex because of additional complexity arising from implementation of nc-Si density of states and nc/mc HJ concept.

In this work, we focus on the accurate modelling of nc-Si/mc-Si HJs by the Medici 2D device simulator [13], and then assess the negative effects of GBs on the device performance without resorting to analytical models. Energy-band structure, I–V and SR of HJ solar cells are studied in the presence of GBs using Medici 2D device simulator. HJ diodes and solar cells were fabricated and characterized to reveal GB effects.

2. The grain boundary in multicrystalline silicon

The GB in a mc-Si substrate constitutes an interface between two identical crystals of different orientations, decorated with crystallographic and metallic defects. The mismatch in bonding between the two crystal grains results in crystallographic or bonding defects, such as disordered bond angles, dilated or compressed bonds, and broken bonds at the GB. Transition of crystallographic orientation from one grain to another grain is very sharp, but these defects are anticipated for an ultra-thin disordered tissue of silicon, a layer a few atoms thick. While the disorder in the crystal structure due to the GB extends only a few nm, the disorder in the electronic structure in the vicinity of the GB can occupy a wider region.

Bonding defects create localized electronic states within the Si bandgap. In p-type mc-Si, holes are trapped in donor-like localized states, leaving a net positive charge at the GB [14]. In the case of n-type mc-Si, electrons are trapped in acceptor-like localized states, leaving a net negative charge at the GB. In both cases, a band bending (V_B) is formed in the vicinity of the GB preventing the diffusion of majority carriers towards the GB and attracting minority carriers into the GB. In addition, the density of the minority carriers in the GB increases exponentially with increasing band bending; this in turn results in an increased level of SRH recombination in the GB region. In general, in the bulk of the mc-Si substrate, minority carriers within a minority carrier diffusion length from the GB can diffuse towards the GB, thus getting trapped and recombining with trapped majority carriers at the GB.

Figure 1 shows a high-resolution transmission electron microscope image of one of our samples showing a GB in mc-Si that locates under a PECVD-deposited (n^+) nc-Si film. As shown in the figure, the GB region is less than 2 nm thick. Although the GB can be modelled as a thin defective volume (TDV) of silicon tissue with a continuous defect distribution inside the bandgap, such model is not that practical for devices with large dimensions. This is so because the GB region in the model must be less than 2 nm thick to properly represent the GB and definition of such tiny features inside a large device increases the number of mesh points in the simulation environment drastically. A defective surface (DS) model with a continuous defect distribution inside the bandgap is a more suitable approach that properly represents the ultra-thin GB region without imposing limitations on density of mesh points. Here, we take the DS model for modelling GB effects on solar cells. For this model we need three important parameters: (i) defect types (electron/hole traps; acceptor/donor traps), (ii) defect density and (iii) capture cross section of the defects. Here, we take a uniform distribution of defect states inside the bandgap. States below the midgap were taken as neutral hole traps and the states above the midgap were taken as neutral electron traps. The neutral hole traps are positively charged above hole quasi-Fermi level and the neutral electron traps are negatively charged below electron quasi-Fermi levels. This clearly justifies the positive (negative) net charge density at the GB in a p-type (n-type) semiconductor. A very wide range of capture cross sections (10^{-17}–10^{-13} cm^2) have been reported for electrons and holes in Si GBs [15–17]. In this study we take an intermediate value of 10^{-15} cm^2 as capture cross section of electron and hole traps for electrons and holes. Medici uses τ_n and τ_p instead of σ_n and σ_p. τ_n and τ_p are calculated from the following formula:

$$\tau_n = \frac{1}{\sigma_n v_{th} N_{Ti}} \qquad \tau_p = \frac{1}{\sigma_p v_{th} N_{Ti}}, \tag{1}$$

where v_{th} and N_{Ti} are the thermal velocity of carriers and density of the defect states at a certain energy level, respectively. Although we have assumed a continuous density of states within the bandgap of the GB region, Medici discretizes the bandgap up to 50 states and extracts the density of states at each energy level [13]. It uses the SRH trap occupation function for calculating trapped charge densities used in Poisson's equation [13, 18]. The SRH recombination rate model is used in the continuity equation and it is used for finding electron and hole generation–recombination rates in the material [13, 18].

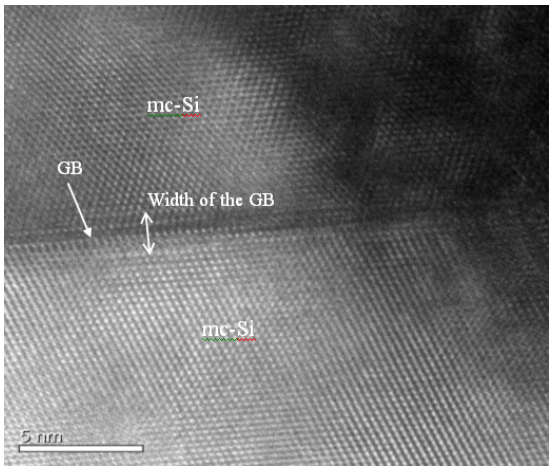

Figure 1. High-resolution TEM image of a GB in the mc-Si substrate (left side). The right side of the image shows a deposited nc-Si film sitting on the GB.

Table 1. Parameters used for the simulations: (a) material parameters of (p) mc-Si and (b) material parameters of the (n^+) nc-Si film.

	(p) mc-Si		
(a)			
Electron affinity (eV)	4.05		
Bandgap (eV)	1.1		
Active doping density (cm^{-3})	10^{16}		
Electron mobility	1000		
Hole mobility	400		
Minority carrier lifetime (μs)	10		
Film thickness (μm)	250		
(b)			
Electron affinity (eV)	3.90	σ_n/σ_p donor-like—tail states (cm^2)	$10^{-15}/10^{-17}$
Bandgap (eV)	1.5	σ_n/σ_p acceptor-like—tail states (cm^2)	$10^{-17}/10^{-15}$
Doping density (cm^{-3})	10^{19}	σ_n/σ_p donor-like–gap states (cm^2)	$10^{-14}/10^{-15}$
Film thickness (nm)	50	σ_n/σ_p acceptor-like—gap states (cm^2)	$10^{-15}/10^{-14}$
G_{D0}, G_{A0} (cm^{-3} eV^{-1})	2×10^{20}	E_A, E_D (eV)	0.01, 0.01
G_{UA}, G_{UD} (cm^{-3} eV^{-1})	2×10^{16}	E_U (eV)—respect to the midgap	0

From a device operation point of view we are mainly interested in the effect of the GB on the device characteristics, i.e., I–V and SR. Therefore, a simpler GB model would be more useful for analysing GB effect at device level without any concern about the defect distribution and parameters. Under a given electrical and optical bias condition the GB can be modelled as a hypothetical sheet (HS) with certain recombination velocities for electrons (S_n) and holes (S_p) and with certain fixed charge density (Q_f). Therefore, we map the DS model into the HS model to reduce the simulation complexity and runtime.

The DS model for a GB was implemented in the middle of a 1 mm long mc-Si strip. Electron traps above the midgap and hole traps below the midgap with density of N_T (cm^{-2} eV^{-1}) have been considered in the simulations. σ_n and σ_p equal to 10^{-15} cm^2 have been chosen for both types of traps. Material parameters of mc-Si have been listed in table 1. Optical excitation was fine tuned to create excess carrier density (Δn) of 10^{12} cm^{-3} and 10^{13} cm^{-3} inside mc-Si material without the presence of GB. These levels of excess carrier density are typical for solar grade silicon absorbers under solar illumination. The structure was simulated in the presence of the GB. S_n was calculated at the edge of the space charge region (SCR) using $J_{GB}/q\Delta n_{SCR}$, where J_{GB}, q and Δn_{SCR} are the current density towards GB at the edge of the SCR, electron charge and excess electron density at the edge of the SCR, respectively. It should be noted that since we calculate S_n from the electron density at the edge of the SCR, Q_f of the HS model must be considered zero. Meanwhile, the charge neutrality principle mandates an equal amount of S_n and S_p for HS model because in QNR and the edge of SCR, assuming a sharp SCR, Δn is equal to Δp and we know that electrons recombine with trapped holes in the GB region. Therefore, in all the simulations regarding the HS model, we consider S_p to be equal to S_n.

Figure 2 shows the correlation between the two models under two different optical bias excitations. This figure shows extracted HS model parameters as a function of the total density of defects at the GB, N_T. The value of S_n strongly depends on N_T in figure 2. Three different regions can be distinguished: (i) $N_T < 8 \times 10^{10}$ cm^{-2}, (ii) $8 \times 10^{10} < N_T < 8 \times 10^{11}$ cm^{-2} and (iii) $N_T > 8 \times 10^{11}$ cm^{-2}. In the first region, band bending varies slowly with N_T because in this regime the defect density is small and its effect on Poisson's equation is negligible because of a relatively large background doping of $N_A = 10^{16}$ cm^{-3}. In this region, the rate of changes in electron density at the edge of the GB is small and S_n is mainly characterized by J_{GB}, which linearly depends on N_T. In the second region, band bending changes much faster than the first region because the total trap hole density in GB is high enough to form a SCR in (p) mc-Si with a doping density of 10^{16} cm^{-3}. The electron density inside the GB varies exponentially with V_B, $n_{GB} = n_{SCR}\exp(V_B/kT)$. Therefore, the SRH recombination rate, which is proportional to n_{GB}, changes rapidly with change in N_T. In this region, J_{GB} still linearly depends on defect density. In the third region, the rate of changes in V_B decreases and J_{GB} saturates at $J_{GB,s} = G_{opt} \times L_n$; therefore the rate of change of S_n versus N_T decreases. It is important to note that J_{GB} is equal to photogenerated carrier loss in a GB, which is equal to short circuit current loss due to the GB.

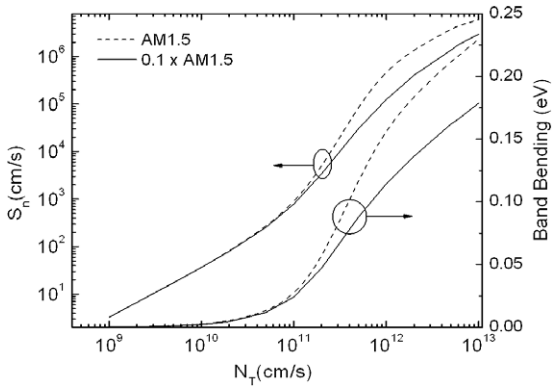

Figure 2. Extracted HS model parameters from the DS model of a GB: S_n and V_B versus N_T considering two different excitation levels $\Delta n = 10^{12}$ cm^{-3} and $\Delta n = 10^{13}$ cm^{-3}.

As shown in the figure, extracted S_n depends on the excitation level and higher excitation level results in a lower S_n. This dependence originates from the decrease in V_B due to the increases in injection level. V_B depends on the net charge

density at the GB and it can be expressed by

$$V_B = \frac{q}{2\varepsilon} N_A W_{SCR}^2 = \frac{q}{8\varepsilon N_A} N_{GB}^2$$
$$N_{GB} = p_t - n_t, \tag{2}$$

where ε, W_{SCR}, N_A, N_{GB}, p_t and n_t are dielectric constant of silicon, width of SCR because of GB, substrate doping density, density of trapped holes in GB and density of trapped electrons in GB, respectively. Under optical or electrical excitation, the quasi-Fermi levels for electrons and holes, Φ_n and Φ_p, split. In a semiconductor out of thermal equilibrium, the neutral electron traps below Φ_n are negatively charged and the neutral hole traps above Φ_p are positively charged. Since E_U locates at the midgap, for Δn larger than the intrinsic carrier density, n_i, and much smaller than N_A, Φ_n locates above E_U and Φ_p remains almost unchanged; therefore, N_{GB} decreases due to the electron trapping at the GB. As a result, V_B and S_n decrease with increasing excitation level.

The HS approximation of the GB in mc-Si solar cells is generally valid. For a mc-Si substrate with an average grain size in mm range and average thickness of about 250 μm, most of the GBs can be considered as 'vertical'. Further, the minority carrier diffusion length is also low (<200 μm) for low-quality mc-Si. Therefore, the current flow through a nc-Si/mc-Si HJ solar cell is expected to be vertical and the current flow across the GB should be negligible. As a result, the GB can be modelled as a hypothetical sheet with certain recombination velocities for minority carriers. In this work, we extracted the HS model from the DS model and then we employed the HS model in 2D device simulations to investigate the effect of GBs on the HJ solar cell characteristics.

3. Modelling of the (n$^+$) nc-Si/mc-Si heterojunction

The bandgap of nc-Si films in a very wide range of 1.1 eV–2.2 eV has been reported using high hydrogen dilutions [19]. Here, we chose a bandgap of nc-Si of 1.5 eV which is an intermediate reported value for nc-Si films. In this paper, (n$^+$) nc-Si is modelled as a semiconductor with an electron affinity (χ) of 3.9 eV and a doping density (N_D) of 10^{19} cm^{-3}. Electron and hole band mobilities (μ_n and μ_p) of 20 cm^2 V^{-1} s^{-1} and 5 cm^2 V^{-1} s^{-1} were chosen to be between the mobility of electron and hole in amorphous and polycrystalline silicon materials. A U-shape gap states defect distribution was employed for modelling gap states. The material parameters of (n$^+$) nc-Si are listed in table 1. For modelling the mc-Si substrate the default silicon parameters in Medici were used. The doping density of the p-type mc-Si (N_A) was considered to be 10^{16} cm^{-3} and the minority carrier lifetime in the mc-Si (τ_n) was assumed to be 10 μs, which is a typical value for low-quality mc-Si substrates, where bulk defects other than grain boundaries can also be present. Figure 3 shows a simulated band energy diagram of an (n$^+$) nc-S/mc-Si HJ diode. The band spikes in conduction and valence bands are 0.15 eV and 0.25 eV, respectively. The SCR width is 360 nm and the built-in potential of the junction is 0.96 V.

Before analysing the effect of GBs on PV characteristics of the HJ solar cells we summarize the main carrier transport mechanisms in a (n$^+$) nc-Si/(p)mc-Si HJ diode [5]. Like other HJs, four different transport mechanisms play a role

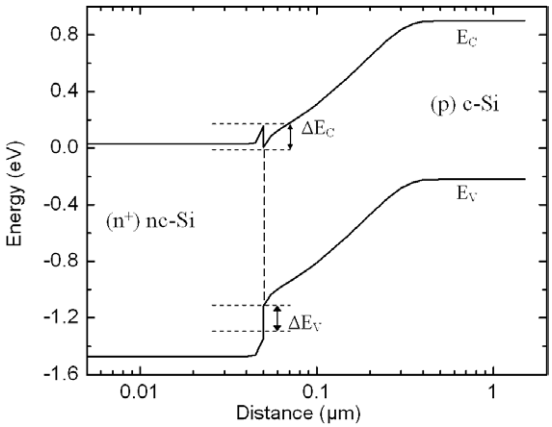

Figure 3. Simulated band energy diagram of (n$^+$) nc-Si/c-Si HJ in logarithmic scale.

in this structure: (i) drift diffusion in SCR, (ii) thermionic emission at heterointerface, (iii) diffusion in the quasi-neutral region (QNR) and (iv) recombination in the heterointerface and space charge region. Basically, carriers move across the SCR by drift diffusion, then are thermionically emitted over the interface energy barrier and then diffuse within the QNR. Since these three transport mechanisms take place sequentially, the slowest process limits the injected current. Meanwhile, the recombination current at the SCR and the heterointerface adds up to this current to form the total current of the diode. For an (n$^+$) nc-Si HJ diode with good interface quality, electrons injecting from (n$^+$) nc-Si into (p) mc-Si do not experience any band spike; therefore the electron current is given by

$$J_n = \frac{q D_n n_{p0}}{L_n}\left(e^{\frac{qV}{kT}} - 1\right), \tag{3}$$

where D_n, L_n and n_{p0} are the electron diffusion coefficient, effective diffusion length and equilibrium electron concentration in (p) mc-Si, respectively. Majority holes in the (p) mc-Si, on the other hand, face a relatively large band spike, 0.25 eV in this structure, to diffuse into (n$^+$) nc-Si. Therefore, a combination of thermionic emission and diffusion in QNR is expected to be the main hole transport mechanism in this structure. As a result the hole current is given by

$$J_p = \frac{J_{ps}}{1 + \frac{S_{dp}}{S_{ip}}}\left(e^{\frac{qV}{kT}} - 1\right)$$
$$J_{ps} = \frac{q D_p p_{n_0}}{K_p} \quad \text{and} \quad S_{dp} = \frac{D_p}{K_p}, \tag{4}$$

where D_p, L_p and p_{n_0} are the hole diffusion coefficient, diffusion length and equilibrium concentration in (n$^+$) nc-Si, respectively. K_p depends on the ratio of the emitter thickness to the hole diffusion length in the emitter (W_n/L_p) and the front contact properties. K_p is equal to W_n if $W_n \ll L_p$ with an ohmic contact at the emitter and K_p is equal to L_p if $L_p \ll W_n$. S_{ip} in (4) is an effective carrier velocity for thermionic emission at the heterointerface and is given by

$$S_{ip} = \frac{A^* T^2}{q N_C} \times e^{-\Delta E_V / kT}, \tag{5}$$

where A^* and ΔE_V are the Richardson constant and the band spike at the valence band, respectively. According to (5),

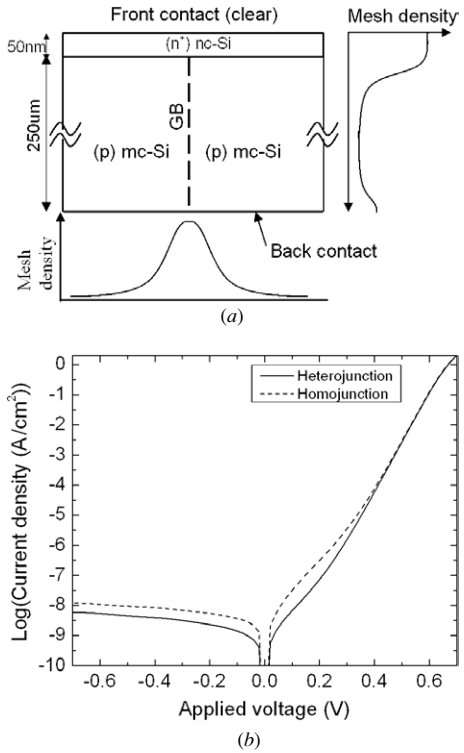

Figure 4. (*a*) Device structure defined in Medici for dark I–V and spectral response simulations. The mesh density was chosen to be high in the nc-Si layer, close to the heterointerface, and close to the GB. (*b*) Dark I–V characteristics of a HJ and a homojunction diode simulated in Medici.

the effective carrier velocity of holes passing the interface depends exponentially on the band spike in the valence band. Therefore, for a small valence band-offset diffusion in QNR and for a large valence band-offset thermionic emission over the heterointerface are the dominant hole transport mechanisms.

Numerical 2D simulation utilizing the material parameters listed in table 1 show that the current transport is mainly due to the recombination current in SCR, in low forward bias regime, and diffusion in QNR, in medium forward bias regime. To simulate the I–V of the HJ diode, the thicknesses of the (n^+) nc-Si and (p) mc-Si were considered to be 50 nm and 250 μm, respectively. The mesh structure is shown in figure 4(*a*). A higher mesh density was allocated to the (n^+) nc-Si film, SCR and back contact regions. For the simulations with the presence of a GB (which we discuss later) a high mesh density was considered in the vicinity of the GB as well. Figure 4(*b*) shows the simulated I–V characteristic of the HJ diode. The I–V characteristic of a classical homojunction diode with the same device structure and material parameters was simulated for comparison.

As shown in figure 4(*b*), the HJ diode behaves exactly like a homojunction in medium and high forward bias regimes as it was expected from (3). Under the low forward bias condition as well as reverse bias the HJ diode results in less saturation current due to the blocking effect band spike in the valence band for holes. In the following section, we investigate the effect of the GB on PV properties of the HJs.

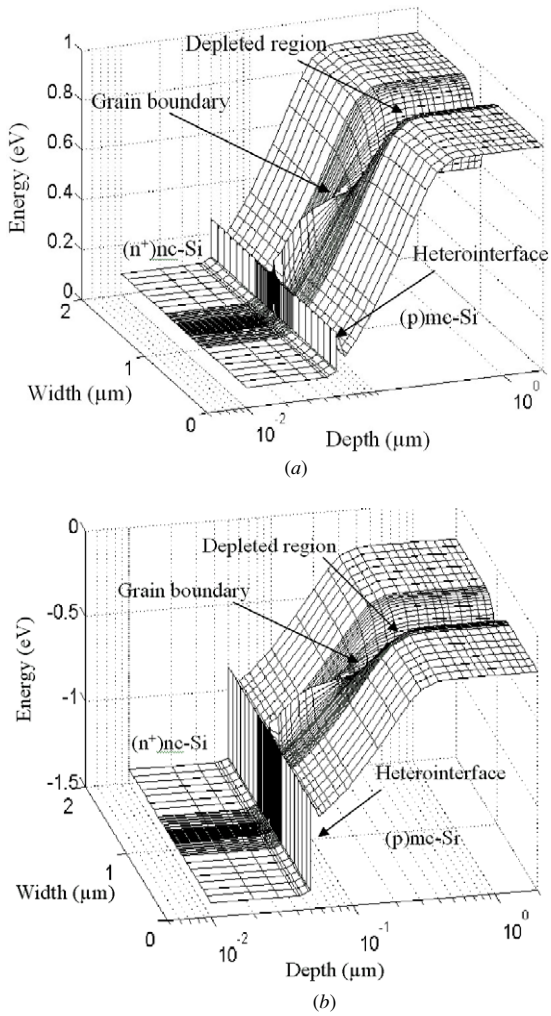

Figure 5. Band energy diagram of (n^+) nc-Si/(p) mc-Si HJ sitting on a GB (*a*) conduction band and (*b*) valence band. The Fermi level in both diagrams locates at 0 eV.

4. Modelling of grain boundary effects in HJ solar cells

4.1. Energy-band diagram

Figure 5 shows the simulated energy-band diagram of the (n^+) nc-Si/mc-Si HJ located on a defective GB without illumination using the material parameters listed in table 1. A DS model of the GB was used with a defect density of $N_T = 10^{12}$ eV^{-1} cm^{-2} and capture cross sections of 10^{-15} cm^2 for all kinds of traps and carriers. The depth axis of the figure far from the GB region is the energy-band diagram of the HJ showing the band offsets at the conduction band, ΔE_C, and valence band, ΔE_V, of 0.15 eV and 0.25 eV, respectively. ΔE_C, which is equal to the difference of electron affinities of silicon and nc-Si, is always in the range of 0.05 eV to 0.25 eV because the reported electron affinities for a-Si and nc-Si all are in the range of 3.8 eV to 4.0 eV. ΔE_V, which is equal to $E_{g,nc\text{-}Si} - E_{g,Si} - \Delta E_C$, on the other hand may experience a large variation due to the deposition parameters because of the large variation in reported electrical bandgap of nc-Si material. Considering $E_{g,nc\text{-}Si}$ in the range of 1.3 eV to 1.8 eV, and assuming ΔE_C of

0.15 eV, ΔE_V in the range of 0.05 eV to 0.55 eV is obtained. Such a large variation in prediction of the valence band makes the prediction of the hole current very difficult. In (n^+) nc-Si/mc-Si HJ we are not concerned about hole transport because electron diffusion in QNR of the (p) mc-Si is the dominant transport mechanism. But such an uncertainty in prediction of the valence band offset may raise serious issues in (p^+) nc-Si/(n) Si HJs.

As shown in figure 5, due to the hole trapping in the GB a SCR is formed adjacent to the GB to compensate GB's positive charge and a relatively large band bending of 0.3 eV is formed far from the interface. As expected, band bending in the dark is larger than the band bending under illumination in figure 2.

Close to the heterointerface inside the SCR, however, electron trapping is dominant because the hole density drops exponentially and electron density grows exponentially in the SCR. However, such behaviour is observed in a thin region of SCR with thickness of less than 0.2 μm adjacent to the heterointerface.

4.2. Dark I–V characteristics

The dark I–V of a HJ solar cell has a great impact on fill factor, open circuit voltage and, hence, on the efficiency of the solar cell. GB defects increase the leakage current, ideality factor and short circuit current loss of the HJ diode. The HS model was employed to assess the impact of GB defects on the dark I–V of the HS diode. The simulated diode has the structure of figure 4(*a*) with a substrate thickness of 250 μm, an nc-Si thickness of 50 nm and a diode width of 200 μm with GB located at the centre. The simulated I–V characteristics, shown in figure 6(*a*), were obtained by changing S_n and S_p as parameters. Three main results can be obtained from this simulation: (i) the dark current of the diode increases with increasing S_n and S_p, (ii) a significant deviation from reference I–V characteristic ($S_n = 0$) of HJ diode is obtained for $S_n >$ 20 000 cm s^{-1} for the simulated device and (iii) recombination at GB affects the low forward bias region more than it does the high forward bias region because of limited minority carrier sinking capacity of the GB. Because of the n^+p HJ with small band offset at the conduction band, the dark current of the HJ diode is mainly due to the electron current. In the forward bias regime, electrons are injected into (p) mc-Si from the (n^+) nc-Si layer. Electrons close to GB, within an L_D from GB can diffuse towards GB and recombine with trapped holes at the GB. Due to recombination at GB, injected electrons experience a small diffusion length in p-type Si. This effect results in a larger minority carrier gradient and a larger diffusion current of electrons in (p) mc-Si. The bias dependence of the GB can be well understood if we note that S_n of the GB has a finite value. At very low forward bias voltages, the density of injected electrons limits J_{GB} while at the large forward bias density the recombination rate and S_n at the GB limit J_{GB}. In other words, under low forward bias conditions, when the injected minority carrier density is less than the recombination rate of minority carrier at the GB, a major part of the injected electrons close to the GB recombine and result in less electron diffusion length and, hence, larger diffusion current. At the high forward bias regime, when the injected electron density in the vicinity of

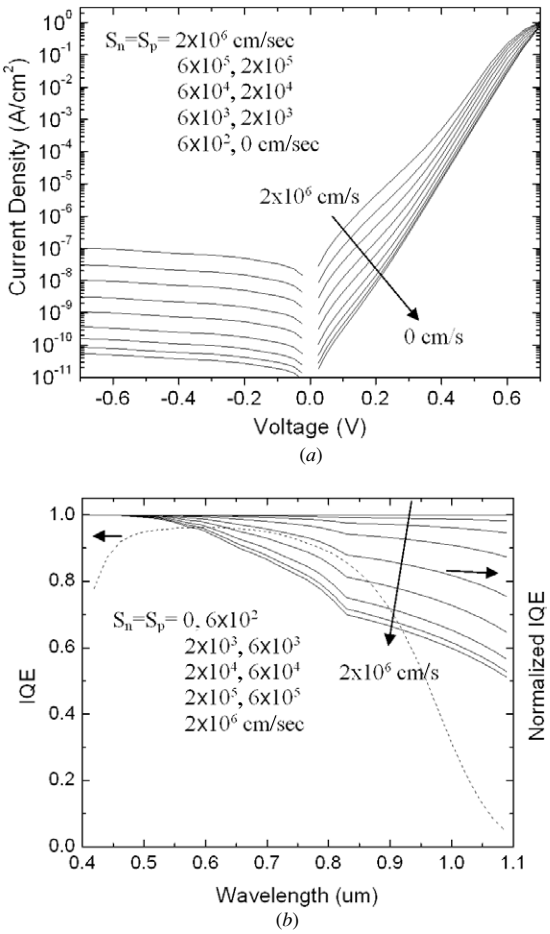

Figure 6. Simulated GB effects on HJ devices for different GB recombination velocities: (*a*) dark I–V characteristics of the HJ diode. (*b*) Internal quantum efficiency of the HJ solar cell. The dotted line shows the IQE of the cell without any GB and the solid lines are normalized IQE with respect to the dotted IQE.

GB is higher than the maximum recombination rate at the GB, most of the injected electrons close to GB do not recombine at the GB. Therefore, the diffusion length of electrons in this case is close to the diffusion length of electrons in bulk mc-Si.

4.3. Spectral response

Spectral response directly shows the photogenerated carrier collection efficiency at the HJ. The structure of figure 4(*a*) with the same parameters used in I–V simulation was employed to simulate internal quantum efficiency (IQE) of the HJ solar cell in the presence of GB recombination. The photogeneration rate was tuned to give $\Delta n = 5 \times 10^{12}$ cm^{-3} in bulk of the mc-Si substrate. Figure 6(*b*) shows the normalized IQE drop because of increasing S_n of the GB using DS model. Normalized IQE is defined as the ratio of $IQE_{on\text{-}GB}$ to $IQE_{off\text{-}GB}$. Simulation results reveal three main points: (i) IQE degrades due to the recombination of minority carriers at the GB. The larger the value of S_n, the less the value of IQE. (ii) IQE is more sensitive to the value of S_n in the range of 6×10^3 cm s^{-1}–2×10^5 cm s^{-1}. (iii) IQE drop due to the GB is wavelength dependent, and low energy photons (photons with long

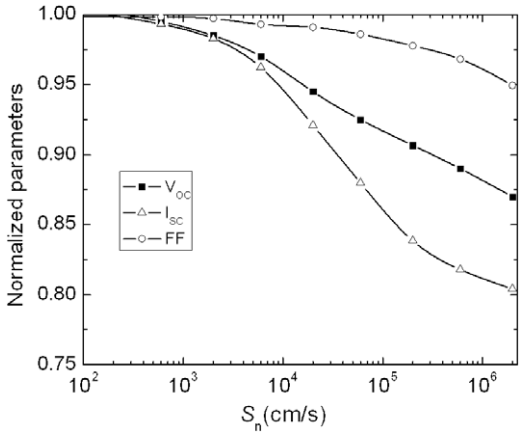

Figure 7. Impact of GB recombination velocity on V_{OC}, I_{SC}, and FF of the simulated HJ solar cell. The illuminated I–V was simulated on the same structure as used for I–V and spectral response simulations.

wavelengths) result in more IQE reduction. This outcome is because the carriers that are photogenerated far away from the junction are more likely to recombine in the neighbourhood of GBs since they need to diffuse longer distances towards the junction. Therefore stronger IQE drop is anticipated at longer wavelengths.

4.4. Illuminated I–V

Illuminated I–V under sunlight is the most important characteristic of a solar cell. We have simulated illuminated I–V of the device using AM1.5 photon flux as an input to the PHOTOGEN command in Medici. Similar to IQE analysis, we take the parameters of the diode with $S_n = 0$ as reference and plot the normalized parameters of other diodes with respect to the reference parameter. Figure 7 shows the impact of recombination velocity of GB on V_{OC}, I_{SC}, FF and η of the solar cell. As shown in the figure, the GB effect starts to show up for S_n values more than 10^3 cm s^{-1} and it becomes significant for S_n values more than 10^4 cm s^{-1}. The negative effect of GB on I_{SC} is more than its effects on V_{OC} and FF. GB has a minor effect on FF but its effect on V_{OC} of the simulated solar cell is noticeable.

5. Experimental details

Test structures of nc-Si/mc-Si HJ devices were fabricated to measure the GB effects. Details of the fabrication process and device characterization are described elsewhere [5]. Two different structures have been fabricated for electrical and photovoltaic characterization: 1 cm^2 HJ solar cells with a Al-SiN/(n$^+$)nc-Si/(p) mc-Si/Al structure where the SiN acts as an anti-reflection coating, and 200 μm × 500 μm HJ diode arrays with a Al/(n$^+$)nc-Si/(p) mc-Si/Al structure.

Dark I–V measurement was performed on several on-GB and off-GB diodes. Figure 8(*a*) shows the test structures for dark I–V measurements. For spectral response measurements a conventional lock-in based spectral response set-up equipped with an optical monochromator and lenses were employed to achieve a narrow monochrome light spot with less than 200 μm width. Micromanipulators were used to align the centreline

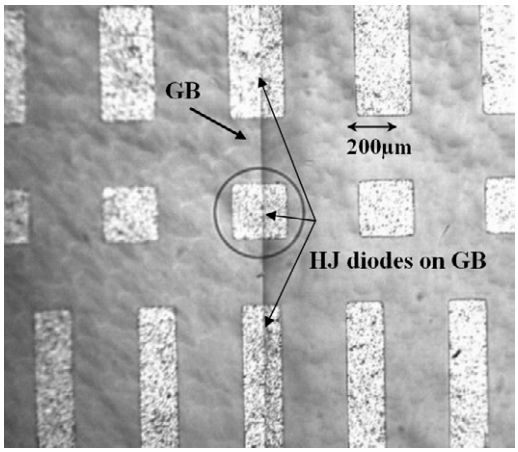

(*a*)

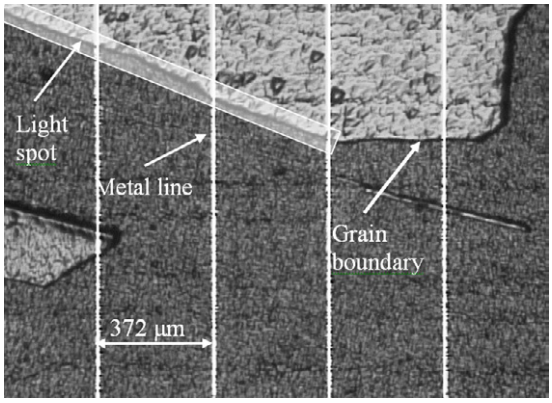

(*b*)

Figure 8. Fabricated HJ (*a*) diodes and (*b*) solar cells located on- and off-GB.

of the light spot on a GB. Figure 8(*b*) shows the alignment process of light spot on a GB.

5.1. Dark I–V characterization

The dark I–V characteristics of mesa etched, on- and off-GB, HJ diodes were measured. The measurements showed consistently inferior I–V due to GB. Figure 9(*a*) shows dark I–V characteristics of two adjacent HJ diodes, one on- and the other one off-GB. As shown, the current level of the on-GB diode is higher than the current of the off-GB diode in the low forward bias regime. More importantly, the saturation current density and ideality factor of the on-GB diode in the medium forward bias, 2.26×10^{-11} A cm^{-2} and 1.13, are larger than those of the off-GB diode, 1.04×10^{-11} A cm^{-2} and 1.07. Such a behaviour, especially in the medium forward bias region, was seen in many measurements. Therefore, we believe that this degraded dark I–V, especially in a medium forward bias regime, originates from the GB effect. Comparing the measured dark I–V of figure 9(*a*) with the modelled dark I–V in figure 6(*a*), a surface recombination velocity of S_n = 7100 cm s^{-1} was obtained for this GB. Due to their small size, there was a peripheral leakage current in the experimental devices at low voltage bias (<300 mV). Therefore only higher voltage bias regions were used for comparison with the simulated curves.

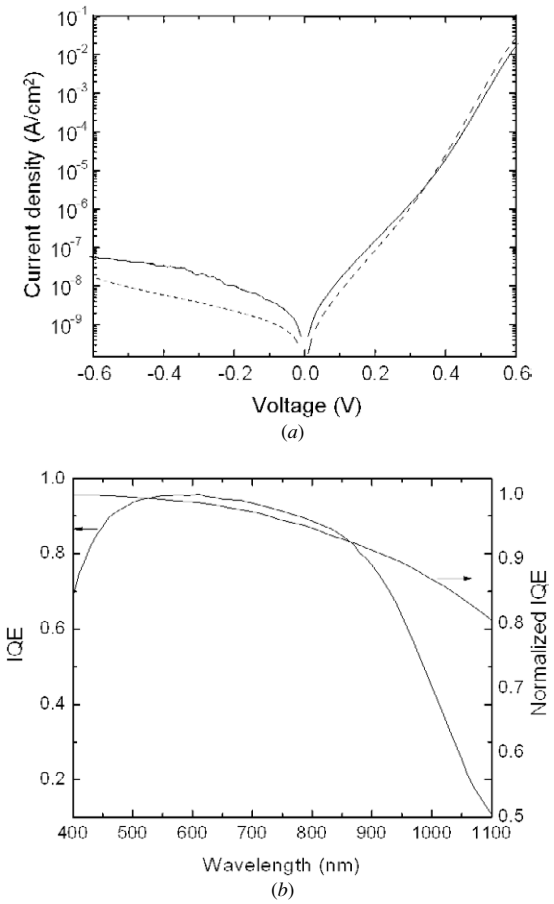

Figure 9. Measured characteristics of the fabricated nc-Si/mc-Si HJ devices: (*a*) dark I–V characteristics of 200 μm × 500 μm HJ diodes on-GB (solid line) and off-GB (dashed line). (*b*) IQE of HJ solar cells on- and off-GB. The on-GB IQE is shown normalized to the off-GB IQE.

5.2. Spectral response

The IQE of 1 cm^2 HJ solar cells was measured inside grains and on the GBs. A section of a 1 cm^2 solar cell in figure 8(*b*) shows GBs, metal grids and the size of the narrow light spot covering a part of GB. IQE measurements on different PV cells showed consistent reduction in IQE due to recombination in GB. The IQE reduction, measured in different samples at 900 nm, is between 8% and 15% for a light spot width of 200 μm and a length of 1 mm aligned on GB. This means that S_n in GB of the employed mc-Si wafer lies in 6000–20 000 cm s^{-1} range. Figure 9(*b*) shows the IQE of an off-GB HJ solar cell and measured GB effect. The normalized IQE in figure 9(*b*) is defined as the ratio of IQE on-GB to IQE off-GB. Comparing measurement and simulation results, we find that the normalized IQE in figure 9(*b*) is in good agreement with the normalized simulated IQE in figure 6(*b*) with $S_n = 11\,500$ cm s^{-1}.

6. Conclusion

The effect of grain boundary on the energy-band diagram, dark I–V characteristics and the spectral response of nc-Si/mc-Si HJ diodes and solar cells were assessed. This study showed that the recombination of photogenerated minority carriers in GBs can affect the spectral response and dark I–V characteristics of the HJ solar cells with small grain mc-Si wafers. Modelling and experimental results reveal three important conclusions: (i) GB effect becomes more critical in the red and infrared regions of the spectral response, (ii) GB effect becomes more critical in reverse bias and low forward bias regimes of the dark I–V characteristics and (iii) recombination velocity of the GB seriously affects the solar cell performance for S_n values more than 20 000 cm s^{-1} for sub-mm range grain sizes. Applying the HS model of the GB to the experimental results, surface recombination velocity of electrons and holes in the range of 6000–20 000 cm s^{-1} were obtained for the mc-Si substrates in this study.

References

[1] Nijs J, Szlufcik J, Poortmans J, Sivoththaman S and Mertens R 1999 *IEEE Trans. Electron Devices* **46** 10
[2] Vyvenko O F, Kruger O and Kittler M 2000 *Appl. Phys. Lett.* **76** 697
[3] Hahn G, Sontag D, Seren S, Schoenecker A, Burgers A, Ginige R, Cherkaoui K, Karg D and Charifi H 2004 *Proc. 19th European Photovoltaic Solar Energy Conf.* p 427
[4] Taguchi M, Kawamoto K, Tsuge S, Baba T, Sakata H, Morizane M, Uchihashi K, Nakamura N, Kiyama S and Oota O 2000 *Prog. Photovolt. Res. Appl.* **8** 503
[5] Farrokh-Baroughi M and Sivoththaman S 2006 *J. Vac. Sci. Technol.* **24** 821
[6] Schmidt W, Woesten B and Kalejs J P 2002 *Prog. Photovolt.* **10** 129
[7] Hahn G, Zechner C, Bitnar B, Spiegel M, Jooss W, Fath P, Willeke G, Bucher E and Hofs H-U 1998 *Prog. Photovolt. Res. Appl.* **6** 163
[8] Ciszek T 1985 *J. Electrochem. Soc.* **132** 963
[9] Seager C H 1982 *Mater. Res. Soc. Symp. Proc.* **5** 85
[10] Ciszek T, Wang T, Burrows R, Wu X, Alleman J, Bekkedahl T and Tsuo Y 1993 *Proc. 23rd Photovolt. Spec. Conf.* p 101
[11] Edmiston S, Heiser G, Sproul A and Green M 1996 *J. Appl. Phys.* **80** 6783
[12] Donolato C 2000 *Semicond. Sci. Technol.* **15** 15
[13] MEDICI User's Manual Version 2001.4, Avant Inc., 2001
[14] McGonigal G, Thomson D, Shaw J and Card H 1983 *Phys. Rev.* B **28** 5908
[15] Murti M R and Reddy K V 1991 *J. Appl. Phys.* **70** 3683
[16] Palm J 1993 *J. Appl. Phys.* **74** 1169
[17] Pecora A, Schillizzi M, Tallarida G, Fortunato G, Reita C and Migliorato P 1995 *Solid-State Electron.* **38** 845
[18] Schroeder D K 1998 *Semiconductor Material and Device Characterization* 2nd edn (New York: Wiley)
[19] He Y, Yin C, Cheng G, Wang L, Liu X and Hu G 1994 *J. Appl. Phys.* **75** 797
[20] http://www.virginiasemi.com/pdf/Optical%20Properties%20of%20Silicon71502.pdf